A STATISTICAL ANALYSIS OF SOLAR FLARE PARAMETERS DERIVED FROM BACKGROUND SUBTRACTED *GOES* DATA OVER THREE SOLAR CYCLES

Daniel Ryan[1], Ryan O. Milligan[2], Peter T. Gallagher[1], Brian R. Dennis[2], A. Kim Tolbert[3], Richard A. Schwartz[1], C. Alex Young[3], & Jack Ireland[3]

Draft version January 12, 2011

ABSTRACT

The GOES catalogue is the largest, self-consistent solar flare listing currently available covering over three solar cycles from 1975 to the present. Solar X-ray flux integrated over the full solar disk is recorded every 3s in each of the two GOES channels (long; 1-8Å and short; 0.5-4Å). By taking the ratio of the flux in the two passbands, parameters of the soft X-ray (SXR) emitting plasma (e.g. temperature (T), emission measure (EM), radiative loss rate etc.) can be derived, as well as the timescales over which they change. However, to date, a self-consistent database of these derived parameters has not been compiled. Previous statistical flare studies have been carried out by Feldman et al. (1996b) using ~800 flares and Hannah et al. (2008) using ~25,000 microflares. However, these studies have either not been self-consistent in how they derived their parameters, or have focused on one particular class of flare. In this paper we outline a method to calculate all plasma parameters for all flares of all classes from 1980-2007 (~60,000 events). This dataset is not only self-consistent, it is larger than any previous dataset of its kind. In compiling such a dataset, it is vital to perform a suitable background subtraction to remove the influence of flux not associated with the flaring plasma. As part of our method we developed a background subtraction technique based on the method described by Bornmann (1990) to account for the non-flaring flux and achieve more accurate results. The work outlined in this paper has laid the foundations for future large-scale self-consistent studies over multiple solar cycles.

1. INTRODUCTION

Solar flares are among the most powerful events in the solar system, releasing up to 10^{32} ergs in a few hours or even minutes. Solar flares are believed to be powered by magnetic reconnection; a process whereby potential energy stored up in coronal magnetic field lines is suddenly released causing the acceleration of particles and the emission of electromagnetic radiation from radio to X-ray wavelengths.

The CSHKP model of solar flares (Carmichael 1964; Sturrock 1966; Hirayama 1974; Kopp & Pneuman 1976) explains many of the key observed features which are a direct (or indirect) result of magnetic reconnection. Magnetic reconnection in a coronal current sheet results in the acceleration of electrons to near-relativistic energies. These particles then propagate along the newly-connected field lines to the chromosphere where they lose their energy by either Coulomb collisions or thick-target bremsstrahlung. The bremsstrahlung emission is observed as hard X-rays (HXR) which can be used to diagnose the properties of the parent electron population while the Coulomb collisions result in the heating of the chromospheric plasma. As the pressure of this heated material is greater than that of the ambient corona, it rises, filling the overlying loops and emitting extreme ultra-violet (EUV) and soft X-ray (SXR) radiation. This process is known as chromospheric evaporation. How-ever, the energy released in the corona can also directly heat the local plasma to high temperatures, which in turn generates a temperature gradient relative to the chromosphere. This again results in chromospheric evaporation but driven by thermal conduction as opposed to a beam of nonthermal electrons. Of course, both mechanisms may take place at the same time with one or the other dominating.

While detailed studies of individual events have furthered our understanding of the physics that underpin these explosive phenomena, perhaps more can be learned through the systematic analysis of multiple events. There have been several statistical studies of the physical parameters of solar flares over the past few decades. Feldman et al. (1996b) combined results from three previous studies (Phillips & Feldman 1995; Feldman et al. 1995, 1996a) to investigate how temperature and emission measure vary with GOES class, from A2 to X2, for 868 flares. Their work used temperatures derived from the ratio of the He-like ions (Fe XXV, Ca XIX, and S XV) from spectra obtained with the Bragg Crystal Spectrometer (BCS) onboard Yohkoh. These temperature values were convolved with the corresponding GOES data to derive values of the emission measure. They found that power-law relationships existed between GOES class and temperature, and GOES class and emission measure, with larger flares exhibiting higher values.

Battaglia et al. (2005) also found a weak correlation between temperature, derived from GOES data at the time of the HXR peak as measured by the Ramaty High-Energy Solar Spectroscopic Imager (RHESSI; Lin et al. 2002), and GOES class for a sample of 85 flares, ranging from B1 to M6 class (A1 to M6 after background subtraction). The fit to their data points was significantly

[1] School of Physics, Trinity College Dublin, Dublin 2, Ireland
[2] Solar Physics Laboratory (Code 671), Heliophysics Science Division, NASA Goddard Space Flight Center, Greenbelt, MD 20771, U.S.A.
[3] ADNET Systems, Inc., NASA Goddard Space Flight Center, (Code 671), Greenbelt, MD 20771, USA

steeper than that of Feldman et al. (1996b) in part due to their accounting for solar background, but also due to the fact that Feldman et al. (1996b) measured the flare temperature from the time of the SXR peak, rather than at the time of the HXR burst, which is likely to underestimate the peak temperature value. Feldman et al. (1996b) also showed that temperatures derived from BCS measurements are slightly higher than those derived from the GOES data themselves.

Christe et al. (2008) and Hannah et al. (2008) investigated the frequency distributions and energetics of 25,705 microflares (GOES class A–C) observed by RHESSI over five years from 2002 to 2007. From those events for which an adequate background subtraction could be performed (about one third) a median temperature of $\sim$13 MK and emission measure of 3×10^{46} cm^{-3} were found. Hannah et al. (2008), in particular, looked at the temperature derived from RHESSI observations as a function of (background subtracted) GOES class, and found similar trends to the works of Feldman et al. (1996b) and Battaglia et al. (2005).

Garcia (2000) analysed 1120 M and X class flares which occurred between 1976 and 1996. The author used three sets of scaling laws (Rosner et al. 1978; Sylwester 1988; Hawley et al. 1995; Metcalf & Fisher 1996) to derive estimates of spatial and thermodynamic parameters (loop length, loop volume, pressure, density, mass, and thermal energy) from GOES data and compared them to the corresponding temperatures and emission measures. It was found that for M and low X class flares, the maximum temperature was greater than the temperature at the time of peak emission measure by 4.3 MK with this difference increasing for more intense flares. Average maximum temperatures and emission measures for low M and low X classes were found to be 12 MK and $10^{49.35}$ cm^{-3} and 25 MK and $10^{49.9}$ cm^{-3}, respectively.

While each of these studies has provided a great insight into the global properties of solar flares, they each have their limitations. Feldman et al. (1996b), for example, does not subtract the solar background when determining the temperature and emission measure, which can bias smaller events where the background makes up a greater contribution to the flux. Deriving temperatures and emission measures at the time of the peak flux (1–8 Å) is also likely to lead to an underestimate of the true peak values. Previous studies (e.g. McTiernan et al. 1999) have shown that the flare temperature reaches a maximum value before the 1–8 Å peak, during the impulsive phase when the energy deposition of nonthermal electrons, and consequently, the heating rate in the chromosphere is greatest. Conversely, the emission measure peaks later than the 1–8 Å peak, after the reconnected loops have filled with evaporated material. Battaglia et al. (2005), while accounting for solar background and deriving the temperature at the time of the HXR peak, limited their study to a small sample of events (85). Hannah et al. (2008) also accounted for solar background, but limited their study to microflares.

In this paper we attempt to improve upon previous works by deriving flare properties, such as peak temperature and emission measure, from GOES data for the largest possible sample of events ($\sim$60,000 over three solar cycles) while systematically accounting for the so-

TABLE 1
GOES FLARE CLASSIFICATIONS.

GOES Class	Peak flux in the 1–8 Å channel (W m^{-2})
X	$\times10^{-4}$
M	$\times10^{-5}$
C	$\times10^{-6}$
B	$\times10^{-7}$
A	$\times10^{-8}$

lar background. Section 2 describes the GOES instrument and the GOES event list. Section 3 describes the method used for subtracting the background, and Section 4 presents the findings. Section 5 summarizes the conclusions and outlines possible future studies that could take advantage of our large sample.

2. INSTRUMENTATION

2.1. *GOES/XRS*

Since 1976, the National Oceanographic and Atmospheric Administration (NOAA) has been operating a series of satellites known as the Geostationary Operational Environmental Satellites (GOES). 2010 March 4 saw the launch of GOES-15. The primary objective of the GOES satellites is to study terrestrial weather. However, each spacecraft also carries an X-Ray Sensor (XRS) onboard as part of the Space Environment Monitor (SEM) suite of instruments. The XRS measures the spatially integrated solar X-ray flux in two wavelength bands (long; 1–8 Å, and short; 0.5–4 Å) every 3 seconds. The overall design of each spacecraft has remained the same over the years aside from the transition from "spin-stabilized" to "3-axis stabilized" platforms in 1995 starting with GOES-8. For an in-depth explanation of the GOES-8 XRS see Hanser & Sellers (1996). The GOES series has provided a near-uninterrupted catalog of solar activity for over 3 complete solar cycles and the GOES flare classification scheme (Table 1) is now universally accepted.

2.2. *The GOES Event List*

In addition to monitoring the total solar X-ray flux since 1976, a catalog of all solar flares (or GOES events) has been compiled. In order for a solar flare to be included in the GOES event list, it must satisfy two criteria [1]:

1. There must be a continuous increase in the one-minute averaged X-ray flux for the first four minutes of the event in the 1–8 Å channel.

2. The flux in the fourth minute must be at least a factor of 1.4 times the initial flux.

The start time of the event is therefore the first of these four minutes. The peak time is when the flux reaches a maximum and the end of an event is defined as the time when the long channel flux reaches a value halfway between the peak and preflare values.

The top panel of Figure 1 shows the X-ray flux in the two GOES channels for an M1.0 solar flare that occurred on 2007 June 2. The start and end times of the associated GOES event are marked by the vertical dotted and
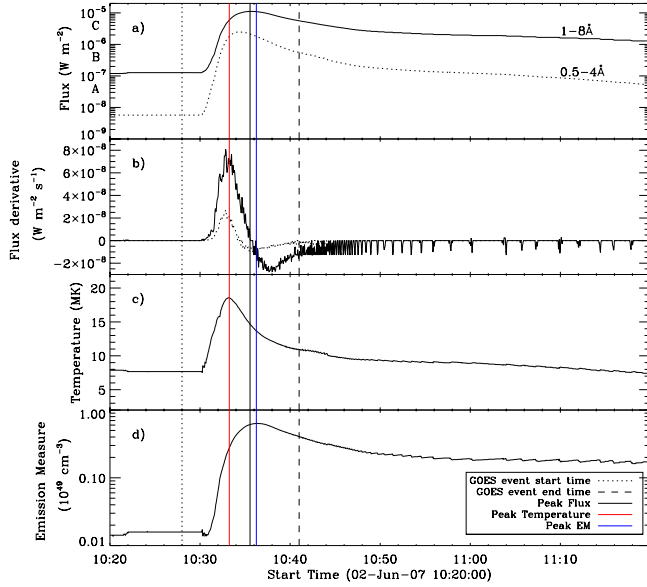
FIG. 1.— X-ray lightcurves of an M1.0 solar flare observed by GOES. *a)* Spatially integrated X-ray flux in each of the two GOES channels (0.5–4 Å; dotted curve and 1–8 Å; solid curve). *b)* First time derivative of the flux in the top panel. *c)* The derived temperature curve. *d)* The derived emission measure curve. The vertical dotted and dashed lines denoted the start and end times of the associated GOES event, respectively. The vertical solid red, black and blue lines mark the times of the peak temperature, peak 1–8 Å flux and peak emission measure, respectively.

dashed lines, respectively. In this case, the end time of the event as defined by the GOES event list is much earlier than the actual end time of the flare, as the X-ray flux remains elevated above the preflare value for many tens of minutes, and often for several hours in larger events.

Figure 1b shows the time derivative of the SXR profiles in the top panel which can often be used as a proxy for the HXR emission under the assumption of the Neupert Effect. The peak in the derivative correlates well with the peak in the temperature (T) profile shown in Figure 1c. This implies that the rate of heating is greatest during the impulsive phase, presumably due to nonthermal electrons as determined from HXR observations (e.g McTiernan et al. 1999). Once the heating has ceased, the flare cools primarily due to thermal conduction resulting from the steep temperature gradients along the flare
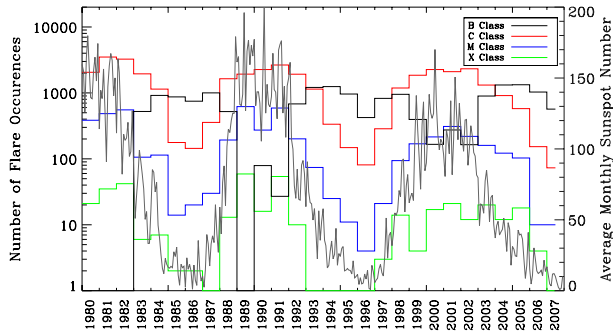

FIG. 2.— Histogram showing the number of flares of a given GOES class as a function of time over the past 2.5 solar cycles. B, C, M, and X class flares are shown by black, red, blue and green curves, respectively. The grey curve shows the average number of sunspots from 1980 to 2007.

loops. Later, the cooling rate decreases and radiative cooling becomes dominant due to the high densities now reached due to chromospheric evaporation (Raftery et al. 2009). This is evident in the bottom panel of Figure 1 which shows the corresponding behavior of the emission measure (EM). This profile peaks later than the peak of the SXR emission as the loops continue to fill with evaporated plasma.

Figure 2 shows a histogram of all the B, C, M, and X class flares recorded in the GOES event list, binned by year, from 1980 January 1 to 2007 December 31. The number of larger flares clearly varies in sync with the sunspot number. The number of B-class flares, however, is anti-correlated with the solar cycle due to the elevated background emission during periods of high activity. This background is often as high as C1.0 level, so that weaker events are not readily detected.

Data from the 1970s were not included in this work due to its poor quality and because many GOES events from this period were erroneously tagged. This meant that a total of 60,424 events, from A-class to X-class, were considered over the time period 1980 January 1 to 2007 December 31. After removing events for which data were unavailable, contained drop outs, or numerous gain changes, 51,779 events remained.

2.3. *Deriving Flare Plasma Parameters*

The X-ray flux, F, measured in either of the two GOES channels can be described by:

$$F \propto G(T, N_e)EM \text{ W m}^{-2} \qquad (1)$$

where $G(T, N_e)$ is the contribution function for an isothermal plasma at temperature, T, and electron density, N_e, and the emission measure, $EM = \int_V N_e^2 dV$. From Equation 1, it is possible to deconvolve the flux value into its constituent components, T and EM, by taking the ratio of the fluxes in the two GOES channels. The derivation of these parameters was first described by Thomas et al. (1985) from polynomial fits to the response of the GOES-1 detectors as functions of temperature. They were later updated by White et al. (2005) for each subsequent GOES spacecraft and incorporated into the SolarSoftWare (SSW; Freeland & Handy 1998) routine GOES_CHIANTI_TEM. These relations are given by,

$$T = A_0 + A_1 R - A_2 R^2 + A_3 R^3 \text{ MK} \qquad (2)$$

$$EM = \frac{F_L}{B_0 + B_1 T - B_2 T^2 + B_3 T^3} 10^{49} \text{cm}^{-3} \qquad (3)$$

where R is the ratio of the flux from each of the two GOES channels ($R = \frac{F_S}{F_L}$; F_S is the flux in the short (0.5–4 Å) channel, F_L is the flux in the long (1–8 Å) channel). For values of the coefficients A_n and B_n for each GOES satellite, see Table 2 of White et al. (2005).

Having determined the temperature and emission measure profiles for a given event, the radiative loss rate and the total radiative losses can be determined. The radiative loss rate, dL_{rad}/dt, is given by,

$$\frac{dL_{rad}}{dt} = EM \times \Lambda(T) \text{ erg s}^{-1} \qquad (4)$$

where $\Lambda(T)$ is the radiative loss function. This is calculated in the SSW routine CALC_RAD_LOSS which uses the most recent version of CHIANTI (version 6.0.1; Dere et al. 2009 spectral models to create a table of radiative loss rate per unit emission measure for various temperatures using the equations outlined in Cox & Tucker (1969) and then interpolates to find the value which corresponds to the flare temperature. The code assumes coronal abundances (Feldman et al. 1992), a constant density of 10^{10} cm^{-3} and the ionization equilibrium from Mazzotta et al. (1998).

Having calculated the radiative loss rate, the total radiative losses, L_{rad}, during the flare can be calculated by integrating over time.

$$L_{rad} = \int_{t_s}^{t_e} \frac{dL_{rad}(t)}{dt} dt \text{ ergs} \tag{5}$$

where t_s and t_e are the start and end times of the GOES event, respectively.

Similarly, the energy losses in the wavelength range of each channel can also be calculated. The X-ray energy loss rate (in a given channel), dL_X/dt, is given by,

$$\frac{dL_X}{dt} = F \times 2\pi d^2 \times 10^3 \text{ ergs s}^{-1} \tag{6}$$

where d is the distance from the GOES satellite to the Sun (1 AU). The total X-ray energy losses, L_X, during the flare can be the be obtained by integration:

$$L_X = \int_{t_s}^{t_e} \frac{dL_X(t)}{dt} dt \text{ ergs.} \tag{7}$$

3. BACKGROUND SUBTRACTION METHOD

As the GOES lightcurves do not contain any spatial information, they contain contributions not only from the flare itself but also from all non-flaring plasma across the solar disk. In order to determine the physical properties of the flare itself, it is essential to subtract the appropriate level of background flux. This is particularly important for weaker events for which the background contribution makes up a larger fraction of the total emission. The two limiting cases are to either assume that the total flux detected by the instrument is dominated by the flare itself, thereby not performing any background subtraction, or estimating the background emission from the preflare level, taken as minimum value of the flux in each channel, usually at the beginning of the event. The first assumption may be valid for events which are orders of magnitude above the background level, but is clearly incorrect for weaker events. The second assumption may be incorrect as there may be significant flare emission before the flare detection algorithm reports the start time.

Examples of pre- and post-background subtracted lightcurves, along with the resulting temperature and emission measure profiles for a B7 class flare that occurred on 1986 January 15 are shown in Figure 3. The profiles in the left-hand column have not had the background subtracted and the middle column profiles have had the preflare flux subtracted. While the bottom two panels of column a in Figure 3 show a believable temperature profile, the corresponding emission measure plot

decreases at the time of the flare. Conversely, by subtracting the minimum value of the flux in each channel, as shown in column b, significant artifacts are introduced because the flux ratio at the beginning of the flare is comprised of two small numbers, which when folded through Equations 2 and 3 result in large discontinuities in the temperature and emission measure profiles.

A more accurate approach would be to assume that the flux from the flare also contains some contribution from the quiescent plasma from which it originates. Figure 4 shows a schematic of a flare lightcurve illustrating this assumption which was the basis for a background subtraction method developed by Bornmann (1990). This technique was used to determine what fraction of the preflare flux (as denoted by the horizontal dashed line in Figure 4) could be subtracted to give physically realistic profiles for the derived properties. An example of this is shown in Figure 3, column c whereby a greater fraction of the preflare flux in the long channel (1–8 Å) was subtracted relative to the short channel (0.5–4 Å). By doing so, the resulting temperature and emission measure profiles do not exhibit any of the erroneous artifacts introduced by subtracting either none or all of the preflare flux, as shown in columns a and b, respectively. Given that each of the two GOES channels measures different energy ranges, it is to be expected that the contribution of the background flux relative to the preflare level will be markedly different also. Given the inherent difficulties associated with subtracting all or none of the preflare flux, as mentioned above, only a certain number of combinations of long and short channel background values will lead to physically meaningful results. The method described in Bornmann (1990) can therefore be adapted to find the most appropriate background level for any given flare.

By dividing the preflare flux level for any given event in each channel into twenty discrete, equally spaced values, 400 combinations of long and short channel background values were generated. This is illustrated in Figure 5 which shows the evolution of the 1986 January 15 flare by plotting the short channel flux against the long channel flux. The grey shaded area represents the region of possible background combinations while the measured fluxes traces out a hysteresis curve. Although this method assumes that the background remains constant during the flare this may not necessarily be the case, especially when the flare occurs during the decay of an earlier event. It was deemed to be rare that this would introduce significant errors especially since the peak flux and peak temperature occur near the beginning of the flare where the background is established.

The technique described by Bornmann (1990) applied three tests to each background combinations described above: the increasing temperature test, the increasing emission measure test, and the hot flare test. These are used to determine whether a given background coordinate produces physically meaningful results. The increasing temperature and emission measure tests (together known as the increasing property tests) assume that both these parameters exhibit an overall increase during the rise phase of a flare, based upon previous spatially-resolved flare observations (references?). The rise phase can then be approximated by a linear fit to
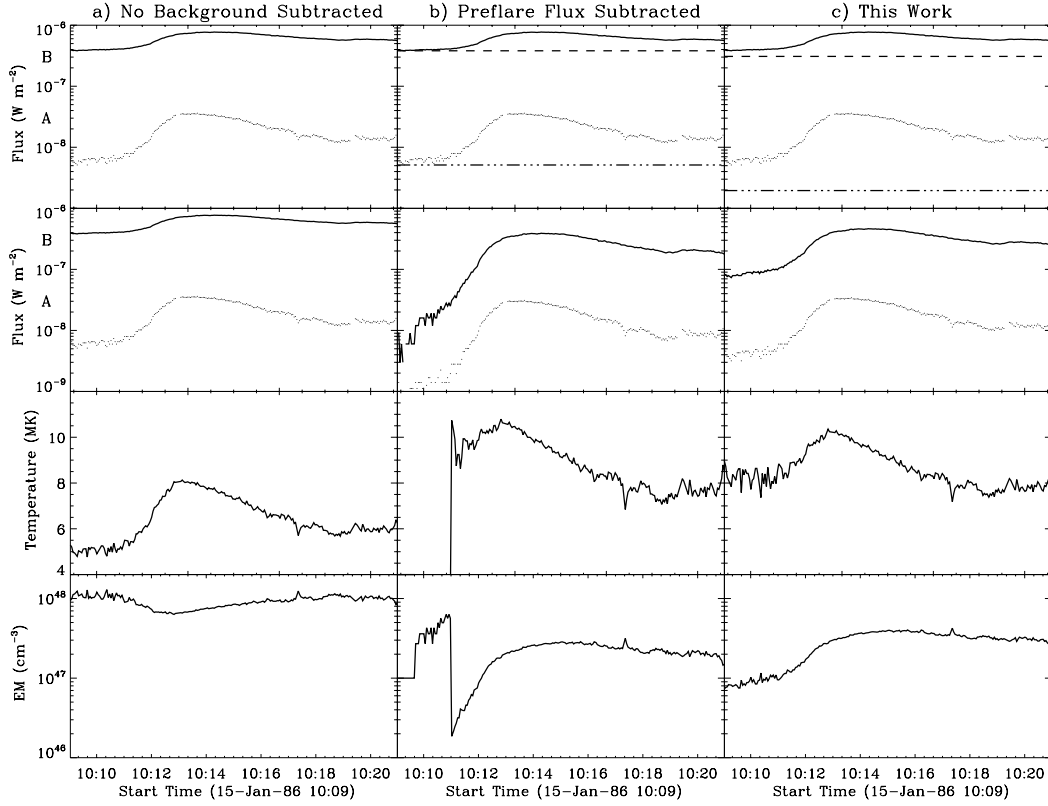
FIG. 3.— Plots of the GOES lightcurves before and after background subtraction, along with the associated temperature and emission measure profiles for the 1986 January 15 flare. The profiles in column *a* have not had the background subtracted. The profiles in column *b* have had the minimum flux value in each channel subtracted, while column *c* shows the profiles obtained using the proposed background subtraction method. The boundaries of the *x*-axis denote the start and end times of the corresponding GOES event.
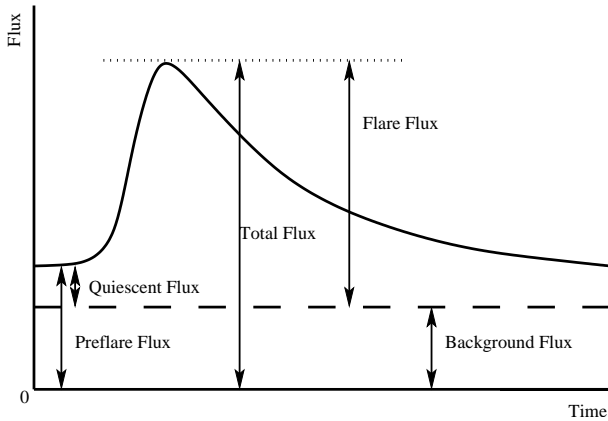

FIG. 4.— Schematic of a flare X-ray lightcurve showing how the total flux detected by (e.g.) the GOES XRS is divided into constituent components. The total flux is the sum of the flux from the flare plus the solar background. The preflare flux, however, is the sum of the background component and the quiescent component of the flaring plasma (e.g. the associated active region; adapted from Bornmann 1990).
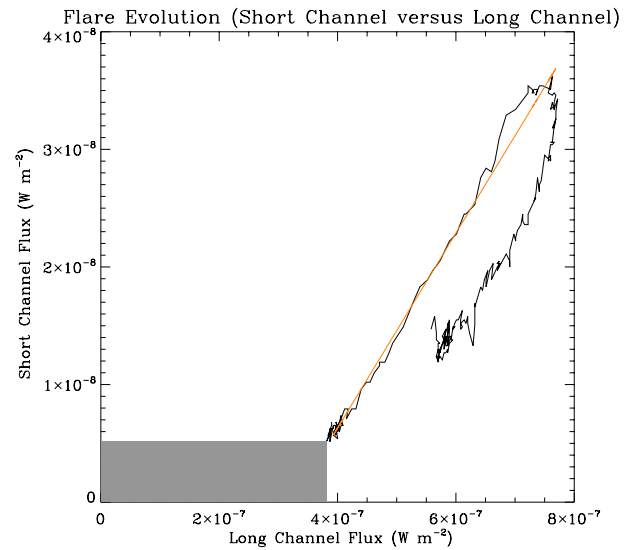

FIG. 5.— Plot of the short channel flux versus the long channel flux for the 1986 January 15 flare (solid curve). The grey shaded area in the bottom left hand corner represents the possible combinations of background values from each channel for this event. The orange line represents a least-squares fit to the rise phase of the event.

the data (as denoted by the straight line in Figure 5) to remove the influence of fluctuations in the data which can skew the results of the increasing property tests. From these fitted values, the temperature and emission measure throughout the rise phase are calculated for each background combination of long and short fluxes. Those combinations that produce consistently increasing tem-

peratures and emission measures are said to pass those tests. Figures 6a and 6b illustrate which background coordinates passed each of the two property tests (solid black = pass, horizontal line = fail). To pass the hot flare

a) Increasing T Test

b) Increasing EM Test

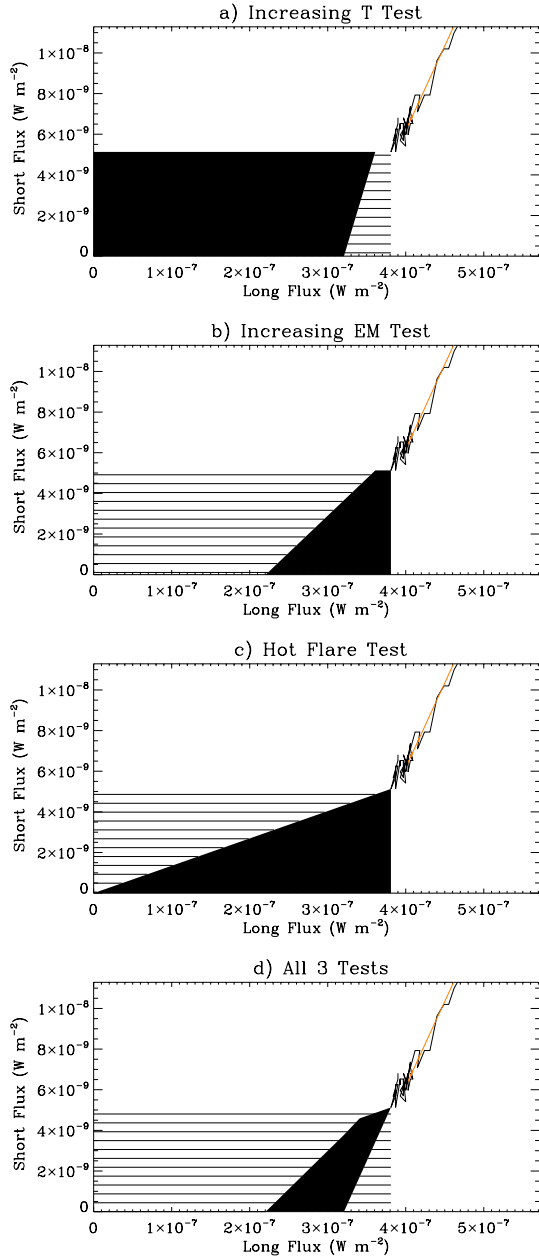c) Hot Flare Test

d) All 3 Tests

FIG. 6.— Plots of the allowed background combinations as a result of each test; the black shaded area illustrates the range of values which pass a given test, while the horizontal line denote background values which fail. a) the increasing temperature test, b) the increasing emission measure test; c) the hot flare test, and d) points which passed all three, or failed one or more.

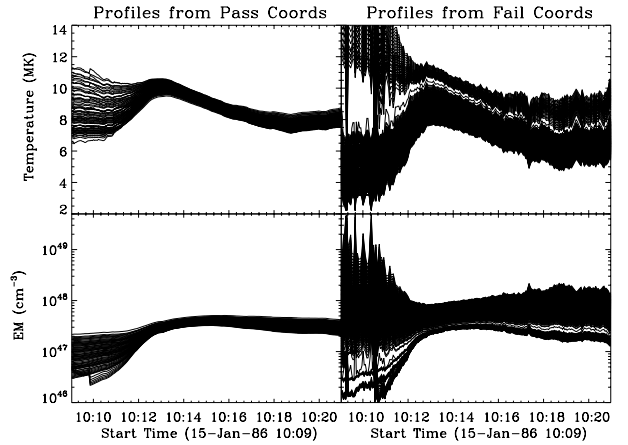Profiles from Pass Coords   Profiles from Fail Coords

FIG. 7.— Temperature and emission measure profiles for the 1986 January 15 flare for all those possible combinations of background levels which passed all three tests (left column), and which failed one or more of the tests (right column).

likely to be emitting more at 1–8 Å than at 0.5–4 Å. Therefore a greater amount of flux will be required to be subtracted at these energies, as shown in Figure 3, column *c*. Figure 7 shows the temperature and emission measure profiles (smoothed for illustrative purposes) calculated from each possible background combinations. The profiles in the left column are from those values which passed all three tests (solid black area in Figure 6d), while those on the right are from the combinations which failed one of more of the tests (horizontal lines in Figure 6d).

4. RESULTS & DISCUSSION

The background subtraction method described in Section 3 was applied to all selected 51,779 flares in the GOES event catalog from 1980 January 1 to 2007 December 31. Of these, successful background subtractions were performed for 39,944 events, and the associated plasma parameters (peak temperature, peak emission measure, total radiative losses, and total X-ray losses in the 1–8 Å channel) were derived. The resulting distributions are plotted as functions of GOES class in Figure 8, along with the corresponding distributions derived by subtracting all or none of the preflare flux for comparison.

The top row of Figure 8 shows the distribution of peak flare temperature as a function of peak long channel flux, or GOES class, for each of the three background subtraction methods used: none, all, and the method of Bornmann (1990). While the non-background subtracted data displays some trend of larger flares exhibiting higher temperatures, there is increased scatter above M-class which displays events with temperatures greater than 25 MK above the main trend of the distribution. In the preflare background subtracted data, there is more scatter, with events of all classes showing temperatures in excess of 25 MK. By subtracting all of the preflare flux, the value of the flux ratio at the beginning of the flare can become erroneously large due to dividing one small number by another. This can further lead to spuriously high temperature values when folded through Equation 2 which can be greater than the real peak temperature of a given event. Many of the high temperature values

test the temperature corresponding to the background combination must be less than the minimum temperature calculated throughout the flare from the background subtracted data. The values which pass and fail this test are shown in Figure 6c. The background combinations which pass and fail all three tests are then shown in Figure 6d.

From this it can be seen that the possible choice of background values in each channel which gives realistic temperature and emission measure profiles has been greatly reduced, more so in the long channel than in the short channel. This is because the solar background is
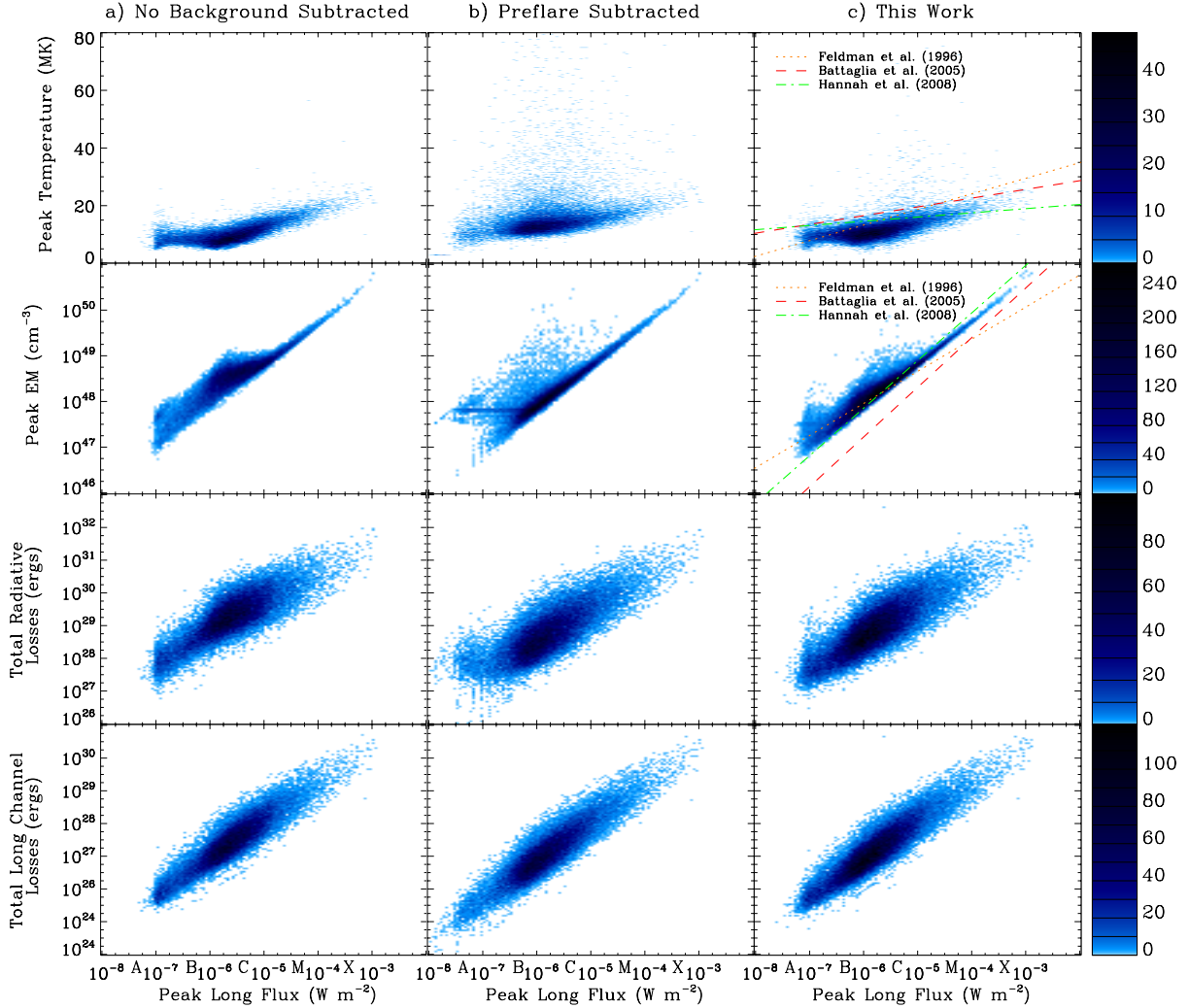
FIG. 8.— Plot showing the distributions of peak temperature, peak emission measure, total radiative losses, and total X-ray losses, each as a function of GOES class, derived using various background subtraction techniques for all selected GOES events observed between 1980 and 2007. The events in the left column had no background subtracted. The events in the middle column had the entire preflare flux subtracted, while the right column shows the distributions using the background subtraction method described in this paper. Overplotted on the right-hand panels are the corresponding relationships derived by Feldman et al. (1996b, orange dotted line), Battaglia et al. (2005, red dashed line), and Hannah et al. (2008, green dot-dashed line).

(> 25 MK) in Figure 8 are taken from such spikes early in the flare which can be found in flares of all magnitudes. The background subtraction method used in this work, keeps these temperature spikes to values smaller be greater than the real temperature peak. As a result the distribution of data points in column *c* shows much less scatter.

This work was compared with previous studies (Feldman et al. 1996b; Battaglia et al. 2005; Hannah et al. 2008). The relations that these studies found are overlaid as dotted, dashed, and dot-dashed lines respectively. This study reveals predominantly lower temperatures for a given peak long channel flux than all three previous studies. There seems to be some agreement with Feldman et al. (1996b) for A- and B-class events but beyond this, higher temperatures are observed. This may be explained by Feldman et al. (1996b) using the BCS to calculate temperature which, as mentioned in Section 1, gives consistently higher temperatures than GOES. There also seems to be close agreement with Hannah et al. (2008)

above M-class. However, this correlation should be regarded with caution since this relation was derived using only small flares. The slope of the relation derived by Battaglia et al. (2005) appears to be closest to that of our distribution but have temperatures 3-4 MK higher. Since the sample of Battaglia et al. (2005) had the least bias toward any given flare class, it is not surprising that this is the case. The discrepancy in the intercept may be explained by a difference in background subtraction methods. If a greater percentage of the short channel is subtracted relative to the long channel, higher temperatures are obtained.

The second row of Figure 8 shows the same plots as mentioned above, but for emission measure as a function of GOES class, rather than temperature. In all cases there appears to be a well defined lower limit to the value of the peak emission measure as a function of GOES class. A similar feature was found by Garcia & McIntosh (1992). The strict upper limits in these cases are a result of the way in which the GOES event list is compiled. The

end of a GOES event is defined in the list as the time at which the 1–8 Å flux falls to half the peak value. The EM can continue to increase beyond this time, particularly for larger events, and hence the value of the EM at the end time of the GOES event corresponds to a lower limit rather than to the true peak value.

Once again the relations derived by Feldman et al. (1996b), Battaglia et al. (2005), and Hannah et al. (2008) have been overplotted with the same line styles as the previous row. There is good agreement with Hannah et al. (2008) across all GOES classes and with Feldman et al. (1996b) at C-class. However, for larger GOES events Feldman et al. (1996b) find lower emission measure. This may be due to the use of the higher BCS temperature values when computing the GOES emission measure. Once again, the slope of the relation found by Battaglia et al. (2005) is very similar to that of this study. However, emission measure values are consistently lower. It was explained above that a different background subtraction can give higher temperature values. Such a background subtraction would also be expected to give lower emission measures. Thus the choice of background values could be the cause of the discrepancy between this study and that of Battaglia et al. (2005).

The third row in Figure 8 shows the distribution of total radiative losses in the 1–8 Å wavelength range as a function of GOES class, something not attempted in previous studies. The distribution shows a clear trend of increased losses due to X-rays at higher GOES classes. Such estimates are useful for estimating the total energy budget of a flare. Emslie et al. (2004) estimated that a flare's total energy was equal to 10 times that of the energy measured by GOES. However, this was later revised to ∼100 times the GOES energy (Emslie et al. 2005) based on total solar irradiance measurements during solar flares by Woods et al. (2004, 2006).

The final row shows the total energy losses through the long channel wavelength range as a function of peak long channel flux. As with relationship discussed in the previous paragraph, a clear increasing trend is observed. Flares with low long channel peaks also have low total losses and vice versa.

Figure 9 shows peak emission measure plotted as a function of peak temperature for the three background subtraction cases displayed in Figure 8. As in the relationships shown in 8, a more discernible trend is revealed by the use of the background subtraction method of this study than in either of the other two cases. The scatter in the distribution of peak EM versus peak temperature is relatively greater than that of the distributions previously studied.

5. CONCLUSIONS & FUTURE WORK

This paper presents a method for subtracting the quiescent solar background from GOES soft X-ray lightcurves in order to systematically derive accurate flare plasma parameters (temperature, emission measure, total radiative losses) for the entire GOES flare catalog. The background subtraction method is based on that described in Bornmann (1990), which assumes that some fraction of the preflare flux is due to the quiescent plasma from which the flare originated. This method requires that, for any given choice of background level in each of the two GOES channels, both the temperature and emission measure must increase during the rise phase of the flare, and that the temperature of the flare at any given time must be greater than that of the background plasma. This approach was found to produce fewer spurious artifacts in the derived temperature and emission measure profiles than when all or none of the preflare flux was removed, in both individual events (Figure 3) and in large statistical samples (Figure 8). These effects were particularly problematic for weak events for which the preflare flux contributed significantly to the overall emission, and for large events which saturated the GOES detectors.

This technique was successfully applied to 39,944 of the selected 51,779 events (A2-X14 background subtracted) from the GOES event list over 2.5 solar cycles. The peak temperature, peak emission measure, and total radiative losses were derived as functions of GOES class (right column Figure 8 and 9). Similar to previous studies (Feldman et al. 1996b; Battaglia et al. 2005; Hannah et al. 2008) it was found that larger flares exhibit higher temperatures and emission measures. Similarly, flares with high temperatures also have higher emission measures (also agreeing with Garcia & McIntosh 1992). These distributions help place constraints on the "allowed" values for a given GOES class, which can be used to help constrain various heating (and cooling) mechanisms. In particular, there appears to be a stringent lower limit on the allowed values of the peak emission measure for all event classes.

This dataset derived from background subtracted GOES data over three solar cycles represents a valuable resource from which to conduct future large-scale statistical analyses/studies of flare plasma parameters, and the timescales on which they vary. For example, Stosier et al. investigated the time delay between peak temperature and peak emission measure as a means of determining loop filling times in multi-stranded versus monolithic flux tube models, but only for 18 events. Aschwanden (2010) recently reported variations in the exponent of the flare frequency distribution, synched to the sunspot number, over 2 solar cycles using HXRBS, BATSE and RHESSI data.

REFERENCES

????

08. 1

Aschwanden, M. J. 2010, ArXiv e-prints

Battaglia, M., Grigis, P. C., & Benz, A. O. 2005, A&A, 439, 737

Bornmann, P. L. 1990, ApJ, 356, 733

Carmichael, H. 1964, NASA Special Publication, 50, 451

Christe, S., Hannah, I. G., Krucker, S., McTiernan, J., & Lin, R. P. 2008, ApJ, 677, 1385

Cox, D. P. & Tucker, W. H. 1969, ApJ, 157, 1157

Dere, K. P., Landi, E., Young, P. R., Del Zanna, G., Landini, M., & Mason, H. E. 2009, A&A, 498, 915

Emslie, A. G., Dennis, B. R., Holman, G. D., & Hudson, H. S. 2005, Journal of Geophysical Research (Space Physics), 110, 11103
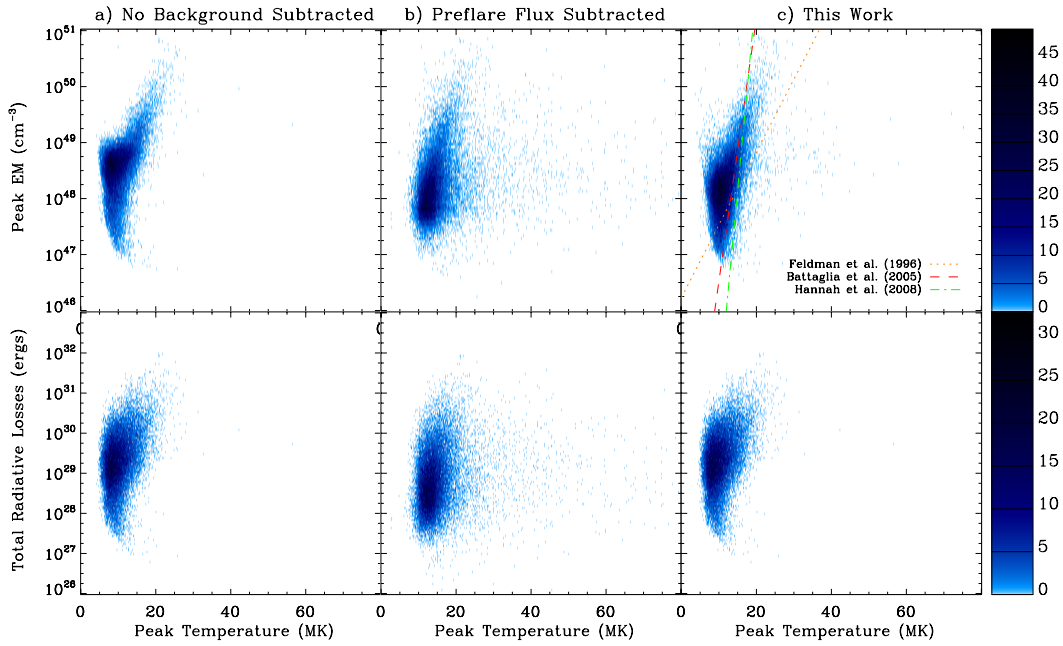
FIG. 9.— Plot showing the distributions of peak temperature versus peak emission measure for each of the three background subtraction techniques. Overplotted on the right-hand panel are the corresponding relationships derived by (Feldman et al. 1996b, orange dotted line), (Battaglia et al. 2005, green dot-dashed line), and (Hannah et al. 2008, red dashed line).

Emslie, A. G., Kucharek, H., Dennis, B. R., Gopalswamy, N., Holman, G. D., Share, G. H., Vourlidas, A., Forbes, T. G., Gallagher, P. T., Mason, G. M., Metcalf, T. R., Mewaldt, R. A., Murphy, R. J., Schwartz, R. A., & Zurbuchen, T. H. 2004, Journal of Geophysical Research (Space Physics), 109, 10104

Feldman, U., Doschek, G. A., & Behring, W. E. 1996a, ApJ, 461, 465

Feldman, U., Doschek, G. A., Behring, W. E., & Phillips, K. J. H. 1996b, ApJ, 460, 1034

Feldman, U., Doschek, G. A., Mariska, J. T., & Brown, C. M. 1995, ApJ, 450, 441

Feldman, U., Mandelbaum, P., Seely, J. F., Doschek, G. A., & Gursky, H. 1992, ApJS, 81, 387

Freeland, S. L. & Handy, B. N. 1998, Sol. Phys., 182, 497

Garcia, H. A. 2000, ApJS, 127, 189

Garcia, H. A. & McIntosh, P. S. 1992, Sol. Phys., 141, 109

Hannah, I. G., Christe, S., Krucker, S., Hurford, G. J., Hudson, H. S., & Lin, R. P. 2008, ApJ, 677, 704

Hanser, F. A. & Sellers, F. B. 1996, in Presented at the Society of Photo-Optical Instrumentation Engineers (SPIE) Conference, Vol. 2812, Society of Photo-Optical Instrumentation Engineers (SPIE) Conference Series, ed. E. R. Washwell, 344–352

Hawley, S. L., Fisher, G. H., Simon, T., Cully, S. L., Deustua, S. E., Jablonski, M., Johns-Krull, C. M., Pettersen, B. R., Smith, V., Spiesman, W. J., & Valenti, J. 1995, ApJ, 453, 464

Hirayama, T. 1974, Sol. Phys., 34, 323

Kopp, R. A. & Pneuman, G. W. 1976, Sol. Phys., 50, 85

Lin, R. P., Dennis, B. R., Hurford, G. J., Smith, D. M., Zehnder, A., Harvey, P. R., Curtis, D. W., Pankow, D., Turin, P., Bester, M., Csillaghy, A., Lewis, M., Madden, N., van Beek, H. F., Appleby, M., Raudorf, T., McTiernan, J., Ramaty, R., Schmahl, E., Schwartz, R., Krucker, S., Abiad, R., Quinn, T., Berg, P., Hashii, M., Sterling, R., Jackson, R., Pratt, R., Campbell, R. D., Malone, D., Landis, D., Barrington-Leigh, C. P., Slassi-Sennou, S., Cork, C., Clark, D., Amato, D., Orwig, L., Boyle, R., Banks, I. S., Shirey, K., Tolbert, A. K., Zarro, D., Snow, F., Thomsen, K., Henneck, R., McHedlishvili, A., Ming, P., Fivian, M., Jordan, J., Wanner, R., Crubb, J., Preble, J., Matranga, M., Benz, A., Hudson, H., Canfield, R. C., Holman, G. D., Crannell, C., Kosugi, T., Emslie, A. G., Vilmer, N., Brown, J. C., Johns-Krull, C., Aschwanden, M., Metcalf, T., & Conway, A. 2002, Sol. Phys., 210, 3

Mazzotta, P., Mazzitelli, G., Colafrancesco, S., & Vittorio, N. 1998, A&AS, 133, 403

McTiernan, J. M., Fisher, G. H., & Li, P. 1999, ApJ, 514, 472

Metcalf, T. R. & Fisher, G. H. 1996, ApJ, 462, 977

Phillips, K. J. H. & Feldman, U. 1995, A&A, 304, 563

Raftery, C. L., Gallagher, P. T., Milligan, R. O., & Klimchuk, J. A. 2009, A&A, 494, 1127

Rosner, R., Tucker, W. H., & Vaiana, G. S. 1978, ApJ, 220, 643

Sturrock, P. A. 1966, Nature, 211, 695

Sylwester, J. 1988, Advances in Space Research, 8, 55

Thomas, R. J., Crannell, C. J., & Starr, R. 1985, Sol. Phys., 95, 323

White, S. M., Thomas, R. J., & Schwartz, R. A. 2005, Sol. Phys., 227, 231

Woods, T. N., Eparvier, F. G., Fontenla, J., Harder, J., Kopp, G., McClintock, W. E., Rottman, G., Smiley, B., & Snow, M. 2004, Geophys. Res. Lett., 31, 10802

Woods, T. N., Kopp, G., & Chamberlin, P. C. 2006, Journal of Geophysical Research (Space Physics), 111, 10